diversity

MDPI

Article

Prokaryotic Diversity and Dynamics during Dinoflagellate Bloom Decays in Coastal Tunisian Waters

Rim Lajnef [1], Marianne Quéméneur [2,*], Moufida Abdennadher [1], Lamia Dammak Walha [1], Asma Hamza [1], Malika Belhassen [1] and Amel Bellaaj Zouari [1,*]

[1] Institut National des Sciences et Technologies de la Mer, 28 Rue 2 Mars 1934, Salammbô 2025, Tunisia
[2] Aix Marseille Univ, Université de Toulon, CNRS, IRD, MIO UM 110, Marseille, France
* Correspondence: marianne.quemeneur@ird.fr (M.Q.); amel.zouari@instm.rnrt.tn (A.B.Z.)

Abstract: (1) Background: Harmful algal blooms (HABs) can negatively impact marine ecosystems, but few studies have evaluated the microbial diversity associated with HABs and its potential role in the fates of these proliferations. (2) Methods: Marine prokaryotic diversity was investigated using high-throughput sequencing of the 16S rRNA gene during the bloom declines of two dinoflagellates detected in the summer of 2019 along the northern and southern Tunisian coasts (South Mediterranean Sea). The species *Gymnodinium impudicum* (Carthage, Tunis Gulf) and *Alexandrium minutum* (Sfax, Gabes Gulf) were identified using microscopy and molecular methods and were related to physicochemical factors and prokaryotic compositions. (3) Results: The abundance of *G. impudicum* decreased over time with decreasing phosphate concentrations. During the *G. impudicum* bloom decay, prokaryotes were predominated by the archaeal MGII group (*Thalassarchaeaceae*), *Pelagibacterales* (SAR11), *Rhodobacterales*, and *Flavobacteriales*. At Sfax, the abundance of *A. minutum* declined with decreasing phosphate concentrations and increasing pH. At the *A. minutum* peak, prokaryotic communities were largely dominated by anoxygenic phototrophic sulfur-oxidizing *Chromatiaceae* (*Gammaproteobacteria*) before decreasing at the end of the survey. Both the ubiquitous archaeal MGII group and *Pelagibacterales* were found in low proportions during the *A. minutum* decay. Contrary to the photosynthetic *Cyanobacteria*, the photo-autotrophic and -heterotrophic *Rhodobacterales* and *Flavobacteriales* contents remained stable during the dinoflagellate bloom decays. (4) Conclusions: These results indicated changes in prokaryotic community diversity during dinoflagellate bloom decays, suggesting different bacterial adaptations to environmental conditions, with stable core populations that were potentially able to degrade HABs.

Keywords: bacteria; archaea; microbial diversity; HABs; dinoflagellates; Tunisia; Mediterranean Sea; marine ecosystems; *Alexandrium*; *Gymnodinium*

Citation: Lajnef, R.; Quéméneur, M.; Abdennadher, M.; Dammak Walha, L.; Hamza, A.; Belhassen, M.; Bellaaj Zouari, A. Prokaryotic Diversity and Dynamics during Dinoflagellate Bloom Decays in Coastal Tunisian Waters. *Diversity* **2023**, *15*, 273. https://doi.org/10.3390/d15020273

Academic Editors: Ana C. Sampaio and Bert W. Hoeksema

Received: 22 December 2022
Revised: 9 February 2023
Accepted: 10 February 2023
Published: 14 February 2023

1. Introduction

Phytoplankton are a major component of marine ecosystems and form the basis of the ocean's food chains. They drive, with the terrestrial biosphere, the chemical composition of the global atmosphere and thereby the climate [1]. They contribute to the production of more than half of terrestrial oxygen [2] and approximately 50% of global primary production. However, under certain conditions, some phytoplankton taxa can grow out of control and form harmful algal blooms (HABs), which can negatively impact aquatic ecosystems and associated economic activities (e.g., aquaculture, fishing activities, and seaside tourism) as well as human health [3,4]. Most harmful microalgae species (planktonic and benthic) belong to the dinoflagellate group, such as species of the genera *Alexandrium* and *Gymnodinium* [5,6], which proliferate recurrently in various marine ecosystems worldwide by forming large blooms in coastal waters [5–7]. Their proliferation can cause contamination and mortality of the seafood chain (including mollusks and fish)

through the production of different kinds of toxins or the creation of anoxic areas by depleting the dissolved oxygen consumed by bacteria during the decomposition of organic matter from microalgae [8].

In recent decades, the increase in the frequency, intensity, and geographical distribution of HABs worldwide has intensified scientific investigations of the ecological and physiological factors that trigger the initiation and the decline of these events and influence their magnitude [9]. HAB dynamics include three critical phases (i.e., the triggering process, maintenance, and decline) and are generally influenced by several synergic abiotic factors, such as hydrodynamic processes, environmental conditions (e.g., temperature, salinity, and vertical mixing turbidity due to wind) [10,11], and nutrient availability [12]. In addition, some biotic factors, such as the compositions of microbial communities, in particular that of bacteria, have been increasingly mentioned as parameters influencing HAB dynamics because of their key roles in biogeochemical cycles and their production of algae-stimulating or -inhibiting elements [13,14]. Bacteria can stimulate HAB growth via nutrient regeneration or vitamin production [15,16] and can induce bloom decay via algicidal activities [17,18]. Recently, it has also been shown that HABs affect bacterial community abundance and diversity [19,20], depending on the type of microalgal species, their physiological state, and the environmental conditions [20,21]. However, the monitoring of archaeal community dynamics during HABs is still largely undervalued [20]. A global consideration of the prokaryotic diversity and the interactions between these microorganisms via an evaluation of their dynamics could improve our understanding of the triggering and resilience mechanisms during HABs and could help in predicting such events.

In Tunisia, the majority of HAB studies have focused on the spatiotemporal distribution of HAB species in relation to abiotic factors, considered as environmental enhancers, such as nutrients and physical parameters (salinity, temperature, and tide amplitude), meteorological constraints (evaporation, air temperature, insolation, rainfall, atmospheric pressure, and humidity), and nutrients [22–28]. Despite their major roles in the functioning of marine ecosystems, no previous data have been collected related to biotic factors, especially the prokaryotic community composition during HABs occurring along Tunisian coasts or other southern Mediterranean coasts.

In this context, the general objective of this study was to analyze for the first time the diversity and dynamics of the marine prokaryotic communities associated with HAB decays in two South Mediterranean coastal ecosystems. Two dinoflagellate bloom events caused by *G. impudicum* and *A. minutum* were, respectively, monitored using microscopy during the summer of 2019 at northern (Tunis Gulf) and southern (Gabès Gulf) Tunisian sites that differed in their functioning and their degree of anthropization/exploitation. Morphology and sequence analyses of ribosomal regions (LSU and ITS) of the *G. impudicum* Gy.imp1 and *A. minutum* Am.6 clonal strains were also investigated. Then, the bloom-forming species were related to environmental variables (i.e., temperature, pH, salinity, and nutrients), and the variability in prokaryotic community composition was investigated using 16S rRNA gene high-throughput sequencing (Illumina MiSeq) to better understand the role of prokaryotes in the decline stages of HABs and potentially propose bioremediation solutions.

2. Materials and Methods

2.1. Study Sites

This study was carried out in two Tunisian coastal sites (southeastern Mediterranean Sea) that were impacted by dinoflagellate blooms during summer 2019 (Figure 1). Since the 1980s, the toxic armored dinoflagellate *A. minutum* has formed many blooms in eutrophic and semi-enclosed ecosystems along the northern (the Gulf of Tunis) [22] and southern (the Gulf of Gabès) Tunisian coasts [23], whereas HAB events associated with *G. impudicum* were observed only in the Bay of Tunis [24–26]. *Alexandrium* blooms have often coincided with mass fish kills [27] and contamination with paralytic shellfish poisoning (PSP) [28].

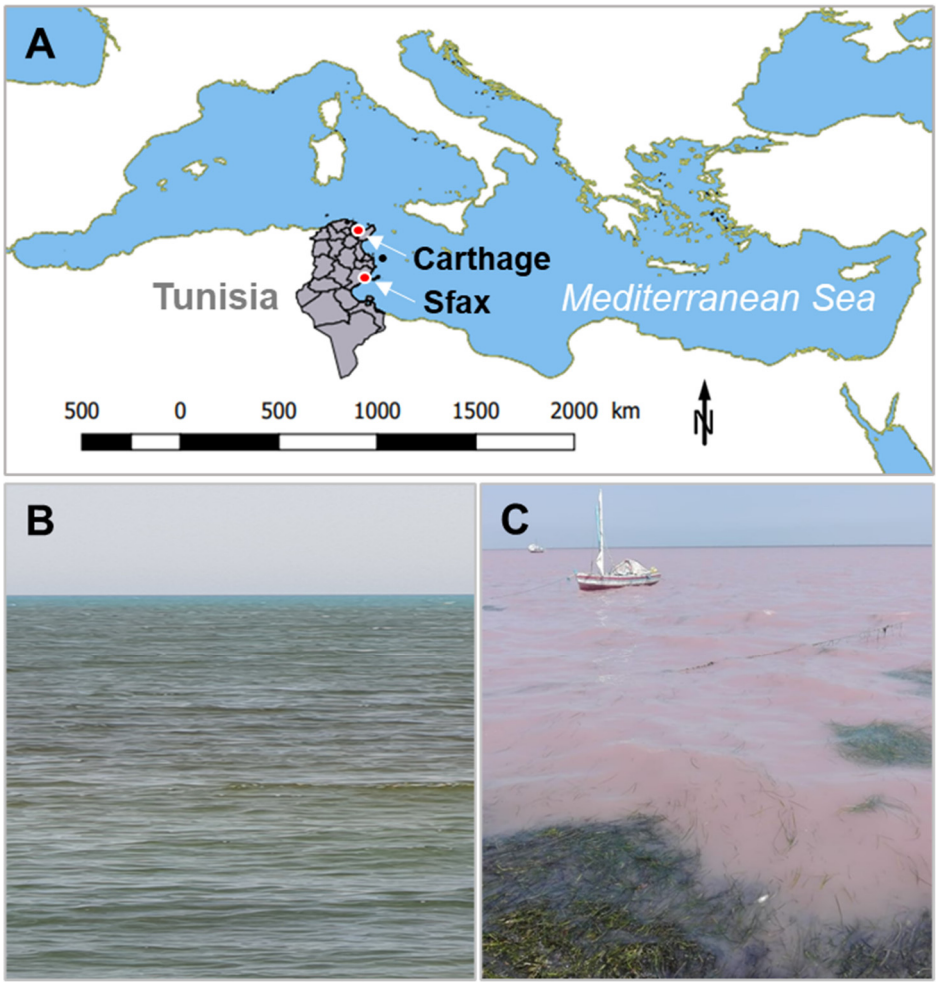

Figure 1. Locations of the sampling sites on the coast of the South Mediterranean Sea. The site of Salammbô is located at Carthage (CAR) in the Gulf of Tunis (northeastern Tunisia), and the site of Sidi Mansour (SM) is located at Sfax on the coast of the Gulf of Gabès (southeastern Tunisia) (**A**). Photographs of brownish (**B**) and red (**C**) seawater discoloration caused by the bloom species *G. impudicum* and *A. minutum* at Carthage and Sidi Mansour, respectively.

The Salammbô site (CAR; 36°83′84″ N, 10°32′03″ E) was in Carthage, one of Tunisia's most important tourist and historic cities, on the Gulf of Tunis (northeastern Tunisia). The sampling site was a bathing area that was impacted by a bloom of *G. impudicum*, a non-toxic chain-forming species, occurring in early July and causing a brown water coloration (Figure 1B). The site of Sidi Mansour (SM; 34°47′55″ N, 10°51′57″ E) was situated on the northern coast of Sfax, Tunisia's second-largest city, in the Gulf of Gabès (south of Tunisia). This gulf is known to display the highest tides in the Mediterranean Sea (up to 2.3 m) [29]. The SM site has been impacted by fishing, trade, harbor activities, and a former phosphogypsum deposit in the Taparura area [30,31]. During the period between the end of June and the beginning of July, this SM site was affected by the red-tide dinoflagellate *A. minutum*, a paralytic shellfish poisoning (PSP)-toxin-producing species (Figure 1C).

2.2. Sampling Procedures

During dinoflagellate blooms, daily sampling was carried out for 4 and 7 days at the Carthage and Sidi Mansour sites, respectively. Seawater samples were collected at a depth of 1 m with a Van Dorn bottle. For microscopic examination, one liter of seawater was fixed with Lugol's iodine solution (4% final concentration). To determine nutrient concentrations (i.e., nitrate (NO_3^-), nitrite (NO_2^-), ammonium (NH_4^+), phosphate (PO_4^{3-}), and silicate (SiO_4^{4-}), 250 mL of seawater was frozen at −20 °C in a plastic bottle that was previously

washed with acid and rinsed with distilled water. Subsamples (250 mL) were filtered in duplicate through a 47 mm diameter membrane filter with a pore size of 0.2 µm, then immediately stored at −80 °C until DNA extraction.

2.3. Dinoflagellate Enumeration, Cultures, and Microscopy Analyses

Cell enumeration was performed using a 10 mL sedimentation chamber under an inverted microscope (Nikon Eclipse TS100) according to the Utermöhl method [32] and was expressed as cells L^{-1} [33]. *A. minutum* and *G. impudicum* cells were isolated from the collected seawater samples using the micropipette technique [34] under an inverted light microscope (Olympus CK40, Tokyo, Japan). Isolated cells were first inoculated into 96-well culture plates (Sigma-Aldrich, St. Louis, MO, USA) in L1 medium [35] and then transferred to a Nunclon culture flask once established (Sigma-Aldrich, St. Louis, MO, USA). Clonal cultures of the *G. impudicum* (Gy.imp1) and *A. minutum* (Am.6) strains were grown at a salinity of 40 in L1 medium at 22 °C on a 12:12 h light/dark cycle with 100 µmol photons $m^{-2}s^{-1}$. Light microscope (LM) observations were performed on living or Lugol-fixed cultured cells using a Carl Zeiss Microscopy GmbH (Jena, Germany) microscope at magnifications of 100, 200, and 400. Images were captured with a Carl Zeiss Axiocam 105 color digital camera and capture software (ZEN core v2.7 acquisition and analysis; Carl Zeiss, Jena, Germany). Cell length (L) and width (W) were measured using images of living cells at magnifications of 200× or 400×. The identification of *A. minutum* was based on thecal plate tabulation [36] following the calcofluor method [37] and using fluorescent brightener 28 (Sigma-Aldrich Co., St. Louis, MO, USA). The cells were examined under 400× magnification in an upright Carl Zeiss Axioimager Z2 Apotome microscope.

2.4. Environmental Parameters and Nutrient Analyses

The temperature, salinity, and pH were measured in situ with a multi-parameter probe (Multi 340i/SET). Nutrient analyses were performed with a BRAN and LUEBBE type III AutoAnalyser using standard methods [38]. Dissolved inorganic nitrogen (DIN) is the sum of the NO_2^-, NO_3^-, and NH_4^+ values.

2.5. Molecular Analyses

2.5.1. DNA Extraction

A DNeasy PowerWater kit (Qiagen, Hilden, Germany) was used to extract DNA from dinoflagellate clonal cultures and planktonic biomass recovered on a 0.22 µm filter, following the manufacturer's instructions with minor modifications. The vortexing time was increased to 10 min, and the DNA elution was performed in a volume of 100 µL. The quality and concentration of DNA extracts were determined using a NanoDrop2000 spectrophotometer (Thermo Scientific, Wilmington, DE, USA). DNA samples were stored at −20 °C until the PCR analyses.

2.5.2. PCR and Sequencing of 16S rRNA Gene Fragments

Bacterial and archaeal 16S rRNA gene V4 variable regions were amplified via PCR using the Pro341F/Pro805R prokaryotic universal primer set [39] with a barcode on the forward primer as previously described by Dowd et al. [40] and were sequenced using the MiSeq Illumina (paired-end: 2 × 300 bp) platform of the Molecular Research Laboratory (Shallowater, TX, USA). In brief, sequences were joined and depleted of barcodes. Then, sequences < 150 bp and sequences with ambiguous base calls removed. Sequences were denoised. Then, operational taxonomic units (OTUs) were generated, and chimeras were removed. OTUs were defined by clustering at 3% divergence (97% similarity). Final OTUs were taxonomically classified using BLASTn against the NCBI non-redundant (NR) reference database. The 16S rRNA gene sequences of dominant OTUs were deposited in the GenBank database under the accession numbers ON195826-ON195869.

2.5.3. PCR and Sequencing of ITS Regions and 28S rRNA Gene

The internal transcribed spacer (ITS1-5.8S-ITS2) regions and the D1–D3 region of the large subunit (LSU) of the ribosomal DNA (28S rDNA) were amplified using PCR with the primer sets ITS1F/ITS1R [41,42] and D1R/D3ca [43], respectively.

Amplification reactions were conducted in volumes of 50 µL each using Go Taq G2 Green Master Mix, 2× (Promega, Madison, WI, USA), 3 µL of DMSO, and 20 ng of genomic DNA as a template under the following program: a denaturing cycle of 3 min at 95 °C; 35 cycles of denaturing at 95 °C for 30 s, annealing for 45 s at 51 °C for the IT1F/ITS1R primers and at 58 °C for the D1/D3ca primers, and extension at 72 °C for 60 s; and a 5 min elongation step at 72 °C was ultimately carried out. The primers ITS1F/ITS1R and D1R/D3ca were used at final concentrations of 0.2 and 0.35 µM, respectively. The purification and sequencing of amplification products were carried out as described previously in the study by Abdennadher et al. [44]. Sequencing reactions were performed with the same primer pairs used for PCR amplification. The nucleotide sequences of ITS-5.8S rDNA and LSU rDNA D1–D3 were submitted to GenBank under the following accession numbers: *A. minutum* Am.6, MZ66321 and MZ489652, respectively, and *G. impudicum* Gy.imp1, MZ366320 and MZ489666, respectively.

2.6. Statistical Analyses

All statistical analyses (Spearman correlations and principal component analyses (PCA)) were performed using XLSTAT 2020.5.1 (Microsoft Excel add-in program; Addinsoft, Paris, France).

3. Results

3.1. Identification of HABs and Cell Abundances

During the HAB monitoring in summer 2019, red and brown tides were observed in Sfax and Carthage, respectively (Figure 1). The dinoflagellate abundance was higher at the Carthage site (impacted by *G. impudicum*) than at the Sfax site (impacted by *A. minutum*) over the sampling period (Table 1). The *G. impudicum* and *A. minutum* cell densities ranged from 2.59 × 10^5 to 33.85 × 10^5 cells L^{-1} and from 0.47 × 10^4 to 30 × 10^4 cells L^{-1}, respectively.

Table 1. Environmental variables obtained at the Sfax (Sidi Mansour (SM)) and Carthage (CAR) sites during the blooms of *Alexandrium minutum* and *Gymnodinium impiducum*, respectively.

Stations	**Sfax (Gulf of Gabès)**							**Carthage (Gulf of Tunis)**			
Samples	SM01	SM02	SM1 [2]	SM2 [2]	SM3 [2]	SM4 [2]	SM5	CAR1 [3]	CAR2 [3]	CAR3 [3]	CAR4 [3]
Sampling Date (dd/mm)	29/06	30/06	01/07	02/07	04/07	08/07	09/07	05/07	06/07	07/07	08/07
Temperature (°C)	32	33	31.2	33	31	34.4	33	25.7	25	25.5	26.1
Air Temp Max (°C)	36	33	31	32	34	39	37	37	39	38	40
Air Temp Min (°C)	23.5	23.5	24	23	24.5	24.5	25	24	22	25	26
Sea-Level Pressure (hPa)	1013	1015	1016	1015	1015	1013	1013	1015.5	1015.52	1013.5	1014.5
Wind Max (km/h)	8	11	21	18	11	9	11	24	15	13	26
Wind Direction (°)	130	137	135	135	135	135	135	23	23	1	180
Day Length (h)	14:29	14:28	14:28	14:26	14:25	14:23	14:22	14:36	14:35	14:34	14:34
Sun Hours	8	8	8	8	7	7	7	13	13	11	10
pH	7.59	7.90	7.95	8.10	8.00	8.23	8.40	7.90	7.95	8.20	8.00

Table 1. *Cont.*

Stations	Sfax (Gulf of Gabès)							Carthage (Gulf of Tunis)			
Salinity (psu)	39.1	39.1	38.8	39.0	38.6	39.1	38.8	37.9	37.8	38.2	37.9
NO_2^- (µM)	0.369	0.912	0.782	0.956	0.391	0.999	0.304	9.281	14.193	15.84	7.651
NO_3^- (µM)	3.21	11.27	8.05	5.02	3.58	15.60	1.95	92.19	114.90	120.40	66.04
NH_4^+ (µM)	96.79	1.72	4.93	6.04	0.89	5.65	44.57	328.08	1283.26	826.51	257.39
PO_4^{3-} (µM)	1.095	0.705	2.074	1.653	0.031	0.063	0.031	11.118	10.465	3.274	1.958
Silicates (µM)	0.721	0.434	2.306	0.757	2.45	0.508	0.577	4.923	5.302	4.292	4.04
DIN (µM) [1]	100.37	13.90	13.76	12.01	4.86	22.25	46.83	429.54	1412.34	962.75	331.09
Microphytoplankton (10^3 cells/L) [2]	300	50	72.2	80	65	10.2	4.7	3385	600	756	259.2

[1] DIN means dissolved inorganic nitrogen (i.e., NH_4^+ plus NO_2^- plus NO_3^-); [2] Microphytoplankton corresponds to the dinoflagellates studied at Sfax (*Alexandrium minutum*) and at Carthage (*Gymnodinium impudicum*); [3] Samples collected for diversity analyses of procaryotic communities.

Morphologically, *A. minutum* cells isolated from the SM site were single, oval to elliptical in a ventral view, and small (Figure 2). Their lengths averaged 23.49 ± 1.72 µm (19.80–27.44 µm, n = 20) and their widths averaged 17.53 ± 1.41 µm (14.3–19.8 µm, n = 20). The main distinctive characteristics described by Halim [45] and Balech [36] are shown, including the presence of a ventral pore at the 1′ right-anterior, the direct connection of the 1′-Po plates, a narrow 6″ plate, and a posterior sulcal plate quadrangular.

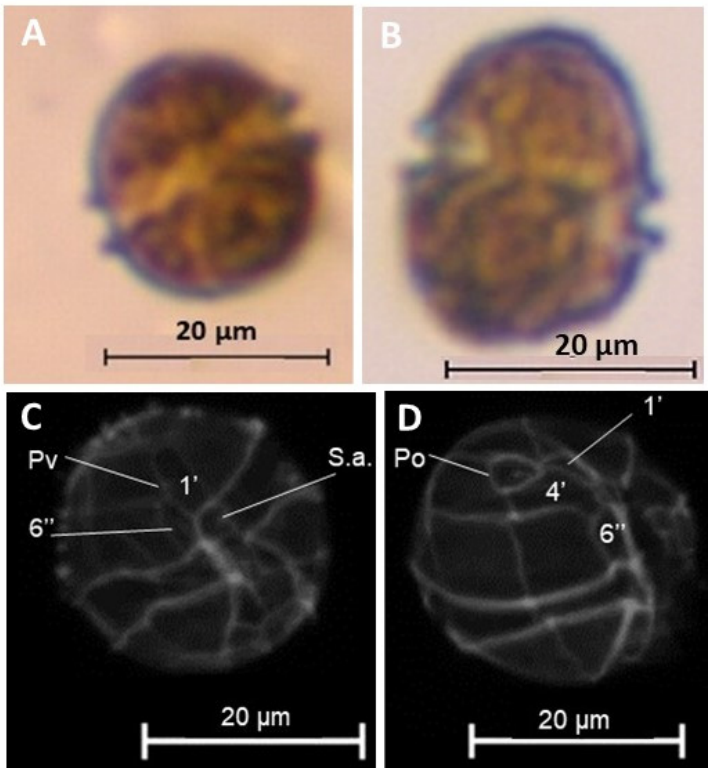

Figure 2. *A. minutum* strain Am.6. (**A**,**B**) Light micrographs (LMs) of living cultured cells. (**A**) LM of dorsal view of cell. (**B**) LM of ventral view of cell. (**C**,**D**) Fluorescence microscopy of CalcoFlour-white-stained cells. (**C**) Ventral view showing the ventral pore (Pv) on the 1′ plate, the narrow 6″ plate, and the sulcal anterior plate (S.a.). (**D**) Lateral view showing the connection between the Po and the 1′ plate.

G. impudicum cells isolated from the CAR site were 23.31 ± 3.27 µm long (18.12–32.07 µm, n = 20) and 18.54 ± 2.05 µm wide (15.19–22.57 µm, n = 20). They often formed chains of four

cells, although longer and shorter chains, as well as solitary cells, were observed (Figure 3). The size of the cells generally grew towards the posterior end of the chain (Figure 3C,D). Numerous banded chloroplasts were located in the cells' peripheries (Figure 3A,D). The intermediate cells in the chain had flattened epicones and hypocones, whereas the apical cells had dome-shaped epicones and flattened hypocones (Figure 3C,D).

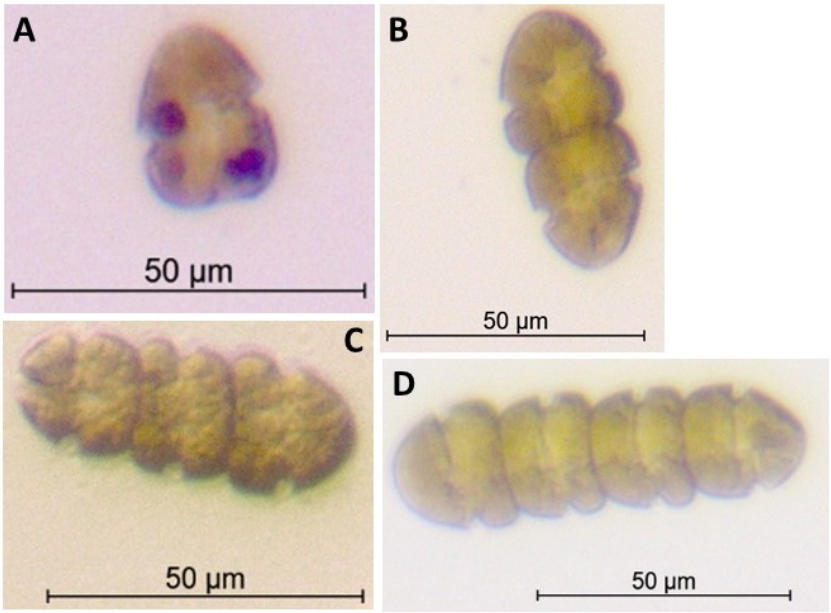

Figure 3. Live cells of *G. impudicum* strain Gy.imp1. (**A**) Single cell showing chloroplasts. (**B**) Ventral view of a pair of cells showing cingular displacement. (**C**) Dorsal view of a chain of three cells in which the posterior cell is much larger than the anterior one. (**D**) Dorsal view of a chain of four cells in which the epicones are clearly larger than the hypocones. The size of the cells increases towards the posterior end of the chain.

Sequencing of both the LSU and ITS regions confirmed the morphological identification of *A. minutum* and *G. impudicum* clonal cultures. The ITS and LSU rDNA D1–D3 nucleotide sequence lengths for Am.6 were 566 and 881 pb, respectively. The sequence lengths were 563 and 949 pb for G.imp1, respectively.

3.2. Environmental Variables and Correlations with HAB Cell Abundances

The physicochemical variables measured at Sfax and Carthage are summarized in the Table 1. During the sampling period, a significant increase in the seawater pH values from 7.59 to 8.40 was observed at Sfax, while at Carthage a lower variation in pH values was detected (ranging between 7.9 and 8.2). The temperature and salinity values for CAR samples ranged from 25.0 to 26.1 °C and 37.9 to 38.2 psu (practical salinity unit), respectively, and were lower than for the SM samples, which ranged from 31 to 34.4 °C and 38.6 to 39.1 psu, respectively. The concentrations of dissolved inorganic nitrogen (DIN, i.e., NH_4^+ plus NO_2^- plus NO_3^-) and phosphate (PO_4^{3-}) in Carthage, ranged from 0.33 to 1.42 mM and from 1.95 to 11.11 $\times$ 10^{-3} mM, respectively, while in Sfax they varied from 4.8 $\times$ 10^{-3} to 0.1 mM and from 0.031 to 2.074 µM.

At Sfax, a negative correlation was observed between *A. minutum* and the minimum air temperature ($r_s = -0.76$; $p < 0.05$), while the abundance of *A. minutum* was positively correlated with the length of the day ($r_s = 0.79$; $p < 0.05$; Table S1). The abundance of *A. minutum* tended to decline over time with decreasing PO_4^{3-} concentrations and increasing pH. The peak bloom concentration of *A. minutum* was also observed at the maximum concentration of DIN (and more specifically at the highest NH_4^+ contents) (Table 1).

At Carthage, no relationship between phytoplankton densities and DIN concentrations was observed during the bloom of *G. impudicum*. However, we noticed that the PO_4^{3-} concentrations decreased during the HAB decline stage (between the bloom's peak stage and the end of sampling, corresponding to the end of the bloom) at both Carthage and Sfax.

3.3. Prokaryotic Community Composition during Dinoflagellate Bloom Declines

Molecular surveys based on a 16S rRNA gene analysis provided evidence of diverse prokaryotic communities in coastal waters during dinoflagellate bloom monitoring. Overall, seventeen different phyla were identified across the seawater samples: Acidobacteria, Actinobacteria, Bacteroidetes, Chlorobi, Chloroflexi, Cyanobacteria, Euryarchaeota, Fibrobacteres Firmicutes, Fusobacteria, Nitrosperae, Planctomycetes, Proteobacteria, Spirochaetes, Tenericutes, Thaumarchaeota, and Verrucomicrobia (Figure 4). Proteobacteria were predominant in all samples (64.8 ± 9.8%, 54.0–83.3%), followed by Bacteroidetes (12.6 ± 2.7%, 10.2–16.8%), Euryarchaeota (7.5 ± 8.6%, 0.1–8.2%), Actinobacteria (6 ± 4.5%, 1.5–14.0%), Cyanobacteria (5.6 ± 4.8%, 0.7–15.6%), and Verrucomicrobia (1 ± 0.8%).

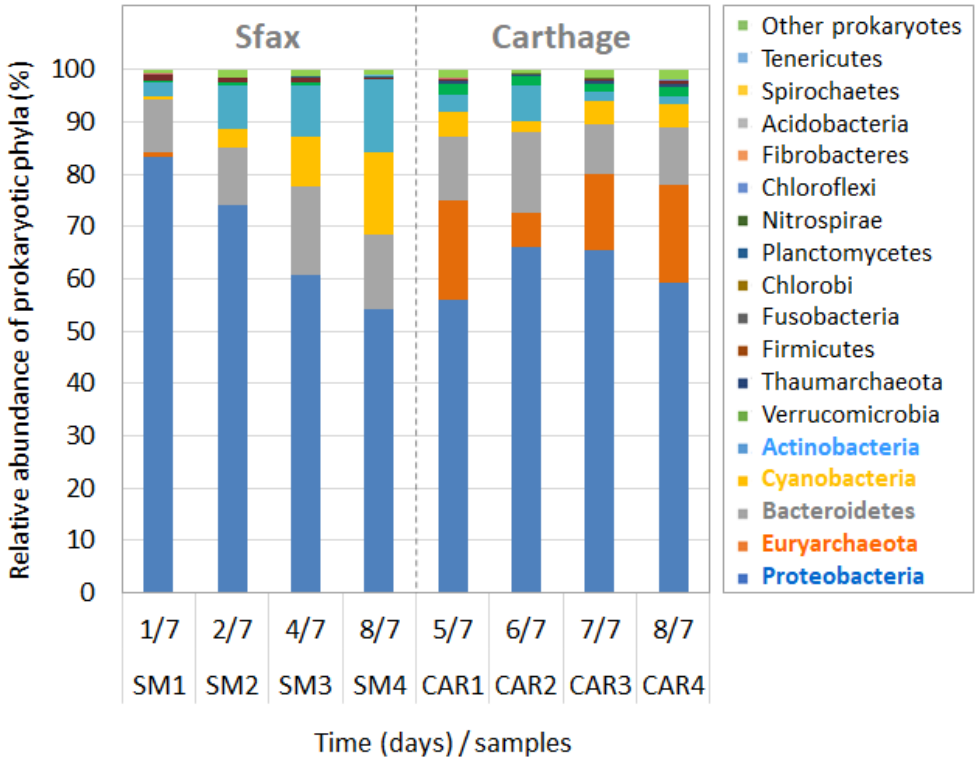

Figure 4. Compositions of prokaryotic communities at the phylum level in the waters of the Sfax site (Sidi Mansour (SM)) and the Carthage site (CAR) during dinoflagellate blooms.

Differences in microbial community composition were observed at different taxonomic ranks between the SM and CAR sampling sites. At the phylum level, the contents of Proteobacteria (>50% on average) and Bacteroidetes (>10%) were similar, but Cyanobacteria and Actinobacteria were more abundant at Sfax than at Carthage (Figure 4). In addition, Euryarchaeota were abundant at CAR (>10–20%) but rare at SM (<1%). Marked differences were observed at lower taxonomic levels, i.e., the order and family levels (Figure 5). The archaeal MGII group (>10%), Pelagibacterales (>10%), Rhodobacterales (>10%), and Flavobacteriales (>5%) clearly dominated at Carthage, while both archaeal MGII and Pelagibacterales were found in lower proportion at SM, with a dominance of Rhodobacterales (Rhodobacteraceae) and Chromatiales (Chromatiaceae).

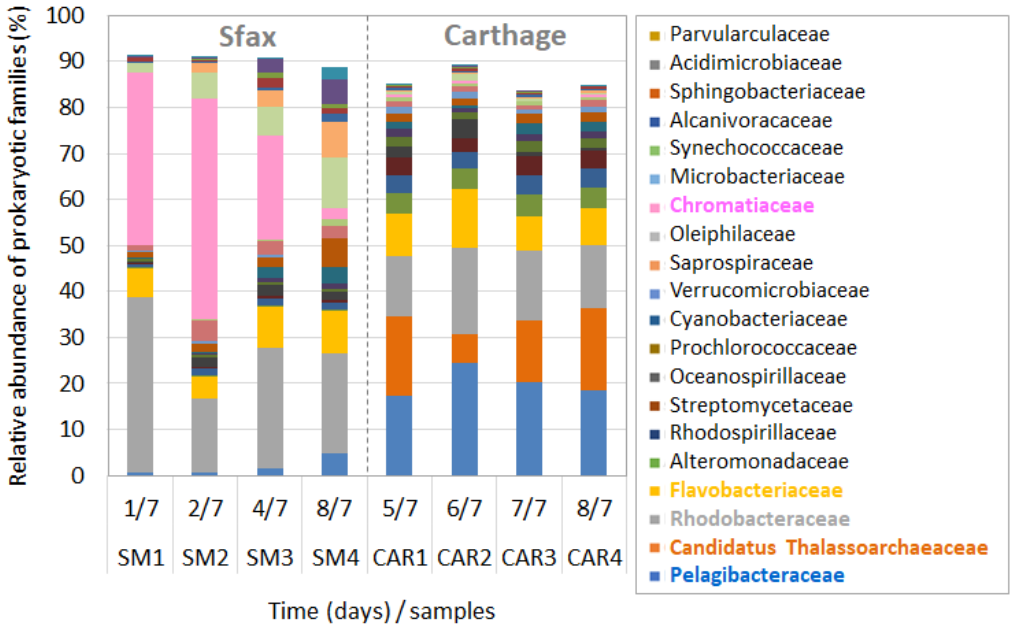

Figure 5. Compositions of prokaryotic communities at the family level in the waters of the Sfax site (Sidi Mansour (SM)) and the Carthage site (CAR) during dinoflagellate blooms.

Pronounced variation in the prokaryotic community structure was also observed at Sfax over the sampling period (Figure 5). At the beginning of the monitoring, Rhodobacteraceae were the dominant bacteria (SM1), but they decreased with the increase in Chromatiaceae at SM2 (47%), the second monitored day, before decreasing progressively to represent only 2–3% of the community at the end of the survey (Figure 5). On the contrary, the prokaryotic diversity at these taxonomic levels was more stable during the decline of the *G. impudicum* bloom at Carthage, but a decrease in *Ca.* Thalassarcheaceae (MGII) with an increase in Pelagibacteriaceae (SAR11) was observed on the second sampling day (CAR2) (Figure 5).

3.4. Dynamics of Abundant Prokaryotic Species during Dinoflagellate Bloom Declines

Three and four OTUs dominated the prokaryotic communities (>5% of total reads) during the progressive declines of *G. impudicum* and *A. minutum*, respectively (Figure 6).

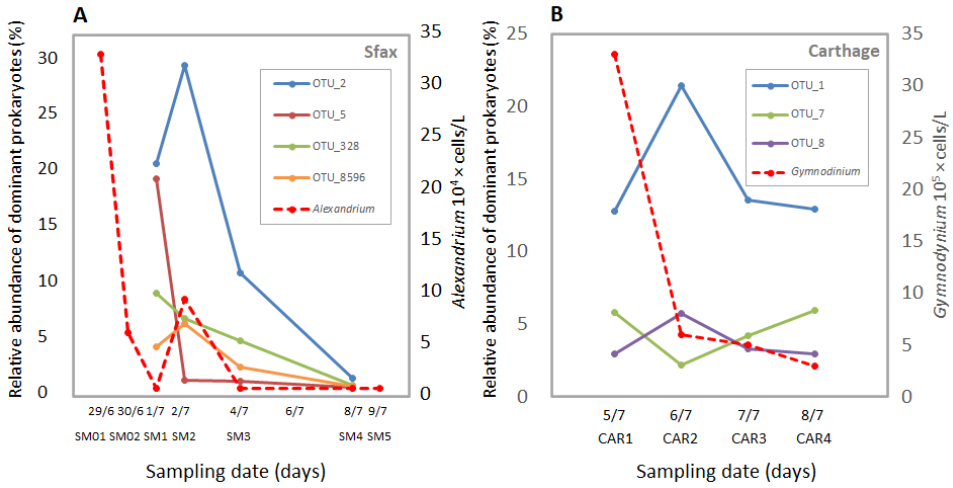

Figure 6. Relative abundances of the dominant prokaryotic OTUs (>5% of total sequences in at least one sample) associated with the abundance of *A. minutum* at the Sfax site (**A**) and *G. impudicum* at the Carthage site (**B**) during the decline phases of their respective blooms occurring in the summer of 2019. The BLAST affiliations of the dominant prokaryotic OTUs can be found in Table S2.

At Carthage, the dominant prokaryotes associated with *G. impudicum* decay were mostly represented by *Candidatus* Pelagibacter (OTU #1, SAR11 subclade Ia, >99% identity) that displayed variations during the monitoring period with an increase directly correlated to the dinoflagellate decrease between CAR1 and CAR2, followed by decline. On the contrary, we observed that *Ca.* Thalassoarchaea (OTU #7, Euryarchaea MGIIb, ~90% identity) increased at the end of the monitoring between CAR2 and CAR4.

At Sfax, the prokaryotic communities associated with *A. minutum* decay were dominated by two main OTUs affiliated with *Rhodovulum adriaticum* (OTU #5, >99% identity) and the *Halochromatium*/*Thiohalocapsa* genera (OTU #2, ~96% identity) (Figure 6 and Table S2). *Rhodovulum* OTU #5 dramatically decreased between SM1 and SM2, while Chromatiaceae OTU #2 increased during the same period before decreasing at the end of the monitoring, corresponding to the disappearance of the red color of the waters.

A PCA was performed to identify the factors that affected the prokaryotic communities during the dinoflagellate decays (Figure 7). The first two principal components explained 87.9% and 84.2% of the variability in the data from Sfax and Carthage, respectively. A Spearman's rank correlation analysis showed positive correlations between the dominant prokaryotes, *A. minutum*, and PO_4^{3-} at Sfax, while no relationship was observed between *G. impudicum* and the dominant prokaryotic OTUs at Carthage, where they were influenced by the DIN concentrations.

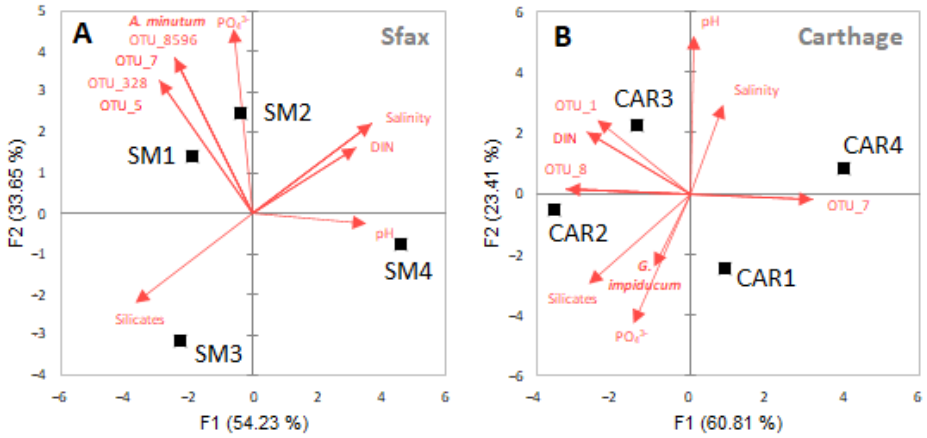

Figure 7. Principal component analysis (PCA) biplots showing the variation among the samples based on the relative abundances of microorganisms and environmental variables. Black squares represent samples from Sfax (**A**) and Carthage (**B**). Arrows indicate the direction of the maximum increase and strength (through the length) of each variable to the overall distribution.

4. Discussion

4.1. HAB Identification and Densities

HABs are usually characterized by the proliferation and occasional dominance of a particular species of toxic or otherwise harmful alga, and in many instances these proliferations discolor the water. Sea surface discolorations vary according to the pigments within the causative species of algae [46,47]. During the summer of 2019, two dinoflagellate species, *A. minutum* and *G. impudicum*, respectively, caused spectacular water discoloration in Sfax (Gabès Gulf) and Carthage (Tunis Gulf).

The *A. minutum* isolated from Sfax largely conformed to the emended descriptions by Halim [45] and Balech [36], with the presence of a ventral pore (Vp.), which has also been observed in several strains of *A. minutum* collected from the Mediterranean Sea [22,48]. The morphological features of the *G. impudicum* strain from Carthage were consistent with previous descriptions, particularly in the production of cell chains [49,50].

The highest abundance of *A. minutum* (3×10^5 cells L^{-1}) observed at Sfax was comparable to other records of *A. minutum* found in the northwestern Mediterranean Sea (10^5 cells L^{-1}) and the North Atlantic coasts (4.6×10^5 cells L^{-1} [51] and 3.3×10^5 cells

L^{-1} [52]. However, relatively higher cell densities (>10^6 cells L^{-1}) have been reported during *A. minutum* blooms on both the Mediterranean and Atlantic coasts [45,53–61]. The highest concentration of *G. impudicum* (33.9 × 10^5 cells L^{-1}) observed in this study was higher than that (2.0–6.3 × 10^5 cells L^{-1}) recorded on the Catalan coast [49] but lower than the highest abundance (71.2 × 10^5 cells L^{-1}) of *G. impudicum* observed in Alexandria (Egypt, southeastern Mediterranean coast) [62].

4.2. Relationships between HAB Species and Environmental Factors

At Sfax, *A. minutum* bloomed at high sea surface temperatures (31–34.4 °C) and salinity (38.6–39.1 psu). However, several studies reported lower temperatures for *A. minutum* cell proliferations, from 12 °C to 24 °C in Mediterranean coastal locations [63] and less than 15° on the Atlantic coasts [52,56]. The salinity tolerance of *A. minutum* is also broad, ranging from 11 [51] to 46 [22] in natural samples. Our observations support the euryhaline and eurythermal character of *A. minutum* species, which has also been demonstrated in culture studies [64,65]. The abundance of *A. minutum* decreased as pH increased, with *A. minutum* peaks at pH 7.6 and the lowest densities at pH 8.4. This finding is consistent with that of Hwang et al. [66] showing higher growth rates of *A. minutum* at pH 7.5 than at pH 8.5. Flores-Moya et al. [67] also found an optimal growth pH of 7.5, with two *A. minutum* strains growing 1.5–1.6 times faster at pH 7.5 than at pH 8. The major nitrogen form, NH_4^+, may have an important role in shaping *A. minutum* blooms on Sfax's northern shore. Accordingly, Maguer et al. [68] demonstrated in experimental research that *A. minutum* preferentially takes up this N form. Field investigations, on the other hand, revealed that nitrate plays a significant role in the development of *A. minutum* blooms [69,70]. The decline in *A. minutum* abundance with decreasing PO_4^{3-} concentrations was consistent with previous field studies showing decreases in cell numbers with decreasing PO_4^{3-} intake [22,69]. Le Bec et al. [70] reported that over 14 years in the Rance macrotidal estuary (Brittany, France), a gradual decrease in phosphorus caused the bloom phenomenon to disappear.

Based on two-year observations, Daly Yahia-Kéfi et al. [26] reported that *G. impudicum* was only observed in the Bay of Tunis during the summer. Here, a *G. impudicum* bloom also occurred in the gulf of Tunis on Salammbô beach (Carthage) during the summer of 2019 (July), with temperatures ranging from 25.0 to 26.1 °C and salinities ranging from 37.9 to 38.2 psu. Previous blooms of this species were also recorded during summer at similar temperatures (22–28 °C) and salinity (36–38 psu) on the northern Mediterranean coasts [58,71] and at much higher temperatures (30.4–32.9 °C) and lower salinity (28.6–29.3 psu) on the southeastern Mediterranean coast [71]. In this study, a decline in *G. impudicum* cell numbers was also observed with decreasing PO_4^{3-} concentrations. Friligos and Gotsis-Skretas [72] reported that *G. impudicum* blooms in the Pagassitikos Gulf (Greece) were linked to pollution and eutrophication. Furthermore, Daly Yahia-Kéfi et al. [26] found that *G. impudicum* blooms appeared in the Bay of Tunis under high PO_4^{3-} levels and nitrogen-limited conditions. Experiments confirmed these field observations; *G. impudicum* uses a wide range of dissolved organic phosphorus compounds in addition to dissolved inorganic phosphorus (DIP). It has been also shown that cultures containing nucleotides (AMP, ADP, and ATP) or phosphomonoesters as well as DIP promote cell growth [73].

Compared to the Sfax site, the Carthage site was very rich in nutrients and had more than 10 h of sunlight with decreasing wind speeds, which could explain why the cell density of microphytoplankton in Carthage was approximately 10 times higher at the bloom peak. The low wind speed and high light intensity may have contributed to the blooms of *G. impudicum* and *A. minutum* in Carthage and Sfax, respectively. These factors tend to affect phytoplankton community structure, dominant species, and biomass. Climatic changes over the past 20 years include a decrease in wind speed [74] and an increase in sun radiation [75]. In fact, light conditions (such as solar radiation and water column transparency) were found to be the most important determinants of phytoplankton community biovolume and structure, which were then followed by the nutrient concentrations and

wind speed [76]. The physical mechanism that best predicts the date of the spring bloom is mixed-layer shoaling, which is characterized by a decrease in wind-driven mixing [77–79]. Accordingly, research by Merlivat et al. [80] in the northwestern Mediterranean Sea (BOUSSOLE site) demonstrated that decreases in mixing and mixed-layer depths caused the start of phytoplankton growth due to wind speed easing after storms. Merlivat et al. [80] demonstrated in the northwest Mediterranean Sea (BOUSSOLE location) that decreases in mixing and mixed-layer depths caused phytoplankton development.

4.3. Taxonomic Composition of the Prokaryotic Community during HAB Decays

In this study, we evaluated the diversity of prokaryotes (bacteria and archaea) associated with *G. impudicum* and *A. minutum* HABs. Several studies have shown that bacteria could play a fundamental role in maintaining [81] or, on the contrary, in the decline of algal blooms [82]. This impact can also be reciprocal, as algal blooms are also known to cause significant changes in planktonic bacterial communities [83–85].

Our monitoring showed that *Proteobacteria* and *Bacteroidetes* were the two major dominant phyla associated with the decline stages of *G. impudicum* and *A. minutum* blooms. Accordingly, Zhou et al. [20] showed that both phyla dominated the prokaryotic community during all stages of the dinoflagellate *Alexandrium catanella*'s spring bloom (northeastern USA, Atlantic Ocean). These authors observed a high proportion of *Bacteroidetes* during the bloom's peak (65.3%), with substantial contents during the post-bloom stages of *A. catanella* (21.5–53.1% versus <20% in our study). As observed at Sfax, they also showed that *Alphaproteobacteria* (*Rhodobacterales*) were predominant during the *Alexandrium* peak and decline stages, suggesting that both *Rhodobacterales* and *Flavobacteriales* (*Bacteroidetes*) may be important regulators of HAB dynamics [86]. Indeed, both photo-autotrophic and -heterotrophic *Rhodobacteraceae* and *Flavobacteriaceae* form a core stable population in Carthage and Sfax waters during dinoflagellate decays and could play important roles in HAB degradation. In addition, Zhou et al. [20] mentioned a predominance of heterotrophic *Gammaproteobacteria,* mainly during the pre-bloom stage of *A. catanella*, while *Chromatiaceae* (Gammaproteobacteria) dominated during the decline of *A. minutum* at Sfax. Together or successively, these bacterial populations belonging to the classes *Alphaproteobacteria*, *Flavobacteriia,* and *Gammaproteobacteria* contribute to the remineralization of the released organic matter during phytoplankton blooms in coastal marine environments [20,86].

In addition to this typical heterotrophic bacterioplankton, the prokaryotic communities associated with *G. impudicum* at Carthage were dominated by *Pelagibacterales* (SAR11) and *Thalassoarchaea* (MGIIb), showing a photoheterotrophic lifestyle. Both cosmopolitan SAR11 and MGII were previously found to be the dominant prokaryotic groups inhabiting coastal Tunisian waters [87]. Here, the relative abundances of the dominant SAR11 and MGII OTUs #1 and #7 displayed opposite variations during the *G. impudicum* decline. According to the work of Pernthaler et al. [88], MGII has been shown to increase in abundance in response to phytoplankton blooms and can account for up to ~30% of the total microbial community after a bloom terminates. Several studies have shown that MGII correlates with specific genera of phytoplankton [89] during and after blooms [90]. Generally, the relative abundance of the two dominant clades of MGII, called MGIIa and MGIIb (the latter is called *Thalassoarchaea)* [90], responds to different environmental conditions, such as temperature and nutrients [91]. *Thalassoarchaea* (MGIIb) populations dominated winter seawater samples, as previously observed in Tunisian seawater [87], whereas MGIIa dominated the prokaryotic community at the beginning of summer. The relative abundance of the class *Thalassoarchaea* in the summer waters at Carthage is thus surprising and could have played an important role in the decline of *G. impudicum*.

4.4. Dominance of Gammaproteobacterial Chromatiaceae during A. minutum Decays

At Sfax, the bloom of *A. minutum* (followed by an increase in the *Chromatiaceae* content during its decline) dramatically modified the typical prokaryotic communities of Tunisian coastal waters analyzed in a previous study [87]. The prokaryotic communities associated

with *A. minutum* decay were dominated by two main OTUs affiliated with alphaproteobacterial *Rhodovulum* (OTU #5) and gammaproteobacterial *Halochromatium/Thiohalocapsa genera* (OTU #2). Here, our results contradicted those of previous studies that used older technologies (plate isolation, DGGE, and FISH) and concluded that the *Rosebacter* genus was the dominant bacterial group associated with *Alexandrium* [92,93]. The high relative abundance of anoxygenic phototrophic sulfur-oxidizing *Chromatiaceae* (also called purple sulfur bacteria (PSB)) may explain the *Alexandrium* decay. In our study, the increase in the PSB proportion (reaching almost half of the prokaryotes at SM2) could be explained by the depletion of dissolved oxygen caused by the dinoflagellate bloom and the development of sulfate-reducing bacteria (SRB) producing sulfide at the Sfax coast sediment surface.

Indeed, the family *Chromatiaceae,* including the genera *Halochromatium* and *Thiohalocapsa*, and SRB are generally abundantly detected in the sediment of the Sfax coast, which is impacted by the release of phosphogypsum, a sulfate-rich coproduct of phosphate-transformation industries [94,95]. Thus, purple sulfur gammaproteobacterial *Halochromatium/Thiohalocapsa* may have also played an important role in intensifying the red color of the Sfax waters during the monitoring period. As observed in our study, Hiraishi et al. [96] showed that red and pink blooms in coastal Japanese environments contained PSB belonging to genera *Thiolamprovum/Thiodictyon* (*Chromatiaceae*) as the major populations, accompanied by smaller but significant densities of purple non-sulfur bacteria, with members of *Rhodovulum* predominating. In addition, red-pink blooms of phototrophic PSB belonging to the family *Chromatiaceae* have also previously been observed during warm summers in shallow brackish coastal lagoons of the Mediterranean coast [97,98], including Tunisian sites [99].

Overall, our study showed a change in the diversity of marine prokaryotes during the decline stages of dinoflagellate bloom events caused by *G. impudicum* and *A. minutum* along the northern (Carthage, Gulf of Tunis) and southern (Sfax, Gulf of Gabes) Tunisian coasts during the summer of 2019. Pronounced differences in the prokaryotic community structure between the waters of the northern and southern Tunisian coasts were previously highlighted during winter observations [87]. In this previous study, *Gammaproteobacteria* were prevalent in the waters of the Gulf of Gabès (near Sfax) but were represented and dominated by different genera, i.e., *Pseudoalteromonas* and *Alteromonas*, which increased with increasing salinity, density, and nutrients (NH_4^+ and/or PO_4^{3-}). The detection of different gammaproteobacterial genera, i.e., *Halochromatium* and *Rhodovulum*, in the present study suggests potential reciprocal interactions between HABs and these bacterial species as well as environmental factors. Temperature and salinity were key environmental factors associated with changes in bacterial and archaeal community structures, respectively, whereas inorganic nitrogen and PO_4^{3-} were associated with eukaryotic variation [20]. According to these authors, temperature was the major abiotic force shaping the microbial community structure in Salt Pond, which was consistent with earlier studies that documented a pronounced impact of temperature on plankton composition [100,101].

5. Conclusions

In this study, the use of high-throughput sequencing of 16S rRNA genes provided a detailed overview of the prokaryotic communities associated with HABs caused by *G. impudicum* and *A. minutum* in the South Mediterranean Sea. To our knowledge, this is the first study evaluating the diversity of the prokaryotic community and its dynamics during HABs occurring along the Tunisian coast and more generally along the southern Mediterranean coast. This study revealed the great influence of dinoflagellate blooms on prokaryotic community structure, with stimulation (e.g., Gammaproteobacteria) or inhibition of specific prokaryotic groups (e.g., Cyanobacteria, SAR11, and MGII), depending on the dinoflagellate species and environmental variables. Dinoflagellate bloom declines stimulated different heterotrophic bacterial taxa, suggesting different abilities to utilize organic matter from dinoflagellates or adaptation to the oxygen depletion caused by dinoflagellate growth.

This study, performed in 2019 and targeting the peaks and declines of dinoflagellate blooms, is currently being continued for several years and includes the pre-bloom phase and more frequent sampling to assess the microbial and abiotic triggers of HABs. Long-term, high-frequency, and in situ monitoring will be necessary to predict and better understand which processes control bloom onset timing.

Supplementary Materials: The following supporting information can be downloaded at https://www.mdpi.com/article/10.3390/d15020273/s1, Table S1: Spearman's rank correlation coefficients (r_s) between the dinoflagellate concentrations and the environmental variables obtained at the Sfax and Carthage sites; Table S2: Blast analysis of the dominant prokaryotic OTUs (>5% of total sequences in at least one sample) obtained from the Sfax (Sidi Mansour (SM)) and Carthage (CAR) sites during dinoflagellate blooms.

Author Contributions: Conceptualization, M.Q., M.B. and A.B.Z.; methodology, R.L., M.Q., M.A., L.D.W., A.H. and A.B.Z.; formal analysis, R.L., M.Q. and A.B.Z.; investigation, R.L. and M.A.; writing—original draft preparation, R.L., M.Q. and A.B.Z.; supervision, M.Q. and A.B.Z. All authors have read and agreed to the published version of the manuscript.

Funding: This research was funded by the Ministry of Higher Education and Scientific Research (Tunisia) and the French National Research Institute for Sustainable Development (IRD).

Institutional Review Board Statement: Not applicable.

Data Availability Statement: The 16S rRNA gene sequences obtained in this study were deposited in the GenBank database under the accession numbers ON195826-ON195869. The ITS-5.8S rDNA and LSU rDNA D1-D3 sequences were deposited in the GenBank database under the following accession numbers: *A. minutum* Am.6, MZ66321 and MZ489652, respectively, and *G. impudicum* Gy.imp1, MZ366320 and MZ489666, respectively.

Acknowledgments: This work was conducted at the National Institute of Marine Sciences and Technologies (INSTM) in the framework of the Tunisian project LittoHABs (HABs in the Tunisian coastline; LR16INSTM04) and under the MOBIDOC scheme, funded by The Ministry of Higher Education and Scientific Research through the PromESsE project and managed by the ANPR. This work was partially supported by the French National Research Institute for Sustainable Development (IRD, the French–Tunisian International Joint Laboratory "LMI COSYS-Med").

Conflicts of Interest: The authors declare no conflict of interest.

References

1. Käse, L.; Geuer, J.K. Phytoplankton Responses to Marine Climate Change—An Introduction. In *YOUMARES 8—Oceans across Boundaries: Learning from Each Other*; Jungblut, S., Liebich, V., Bode, M., Eds.; Springer: Cham, Switzerland, 2018. [CrossRef]
2. Falkowski, P.G. The role of phytoplankton photosynthesis in global biogeochemical cycles. *Photosynth. Res.* **1994**, *39*, 235–258. [CrossRef]
3. Anderson, D.M.; Fensin, E.; Gobler, C.J.; Hoeglund, A.E.; Hubbard, K.A.; Kulis, D.M. Marine harmful algal blooms (HABs) in the United States: History, current status and future trends. *Harmful Algae* **2021**, *102*, 101975. [CrossRef]
4. McKenzie, C.H.; Bates, S.S.; Martin, J.L.; Haigh, N.; Howland, K.L.; Lewis, N.I.; Locke, A.; Peña, A.; Poulin, M.; Rochon, A.; et al. Three decades of Canadian marine harmful algal events: Phytoplankton and phycotoxins of concern to human and ecosystem health. *Harmful Algae* **2021**, *102*, 101852. [CrossRef] [PubMed]
5. Smayda, T.J. Harmful algal blooms: Their ecophysiology and general relevance to phytoplankton blooms in the sea. *Limnol. Oceanogr.* **1997**, *42*, 1137–1153. [CrossRef]
6. Sournia, A. Red tide and toxic marine phytoplankton of the world ocean: An inquiry into biodiversity. In *Harmful. Marine. Algal Blooms*; Lassus, P., Arzul, G., Erard, E., Gentien, P., Marcailou-Le Baut, C., Eds.; UNESCO: Paris, France, 1995; pp. 103–112.
7. Tester, P.A.; Steidinger, K.A. *Gymnodinium breve* red tide blooms: Initiation, transport, and consequences of surface circulation. *Limnol. Oceanogr.* **1997**, *42*, 1039–1051. [CrossRef]
8. Bagatini, I.L.; Eiler, A.; Bertilsson, S.; Klaveness, D.; Tessarolli, L.P.; Vieira, A.A. Host-specificity and dynamics in bacterial communities associated with bloom-forming freshwater phytoplankton. *PLoS ONE* **2014**, *9*, e85950. [CrossRef] [PubMed]
9. Wells, M.L.; Karlson, B.; Wulff, A.; Kudela, R.; Trick, C.; Asnaghi, V.; Berdalet, E.; Cochlan, W.; Davidson, K.; De Rijcke, M. Future HAB science: Directions and challenges in a changing climate. *Harmful Algae* **2020**, *91*, 1016. [CrossRef] [PubMed]
10. Gernez, P.; Antoine, D.; Huotb, Y. Diel cycles of the particulate beam attenuation coefficient under varying trophic conditions in the northwestern Mediterranean Sea: Observations and modeling. *Limnol. Oceanogr.* **2011**, *56*, 17–36. [CrossRef]

11. Lasternas, S.; Tunin-Ley, A.; Ibañez, F.; Andersen, V.; Pizay, M.-D.; Lemée, R. Short-term dynamics of microplankton abundance and diversity in NW Mediterranean Sea during late summer conditions (DYNAPROC 2 cruise; 2004). *Biogeosciences* **2011**, *8*, 743–761. [CrossRef]
12. Anderson, D.M.; Glibert, P.M.; Burkholder, J.M. Harmful algal blooms and eutrophication: Nutrients sources, composition and consequences. *Estuaries* **2002**, *25*, 704–726. [CrossRef]
13. Cui, Y.; Chun, S.J.; Baek, S.S.; Baek, S.H.; Kim, P.J.; Cho, K.H.; Ahn, C.Y.; Oh, H.M. Unique microbial module regulates the harmful algal bloom (*Cochlodinium polykrikoides*) and shifts the microbial community along the Southern Coast of Korea. *Sci. Total Environ.* **2020**, *721*, 137725. [CrossRef]
14. Park, Y.H.; Kim, S.; Kim, H.S.; Park, C.; Choi, Y.E. Adsorption strategy for removal of harmful cyanobacterial species *Microcystis aeruginosa* using chitosan fiber. *Sustainability* **2020**, *12*, 4587. [CrossRef]
15. Higashi, A.; Fujitani, Y.; Nakayama, N.; Tani, A.; Ueki, S. Selective growth promotion of bloom-forming raphidophyte *Heterosigma akashiwo* by a marine bacterial strain. *Harmful Algae* **2016**, *60*, 150–156. [CrossRef] [PubMed]
16. Liu, J.; Lewitus, A.J.; Brown, P.; Wilde, S.B. Growth-promoting effects of a bacterium on raphidophytes and other phytoplankton. *Harmful Algae* **2008**, *7*, 1–10. [CrossRef]
17. Liu, J.; Lewitus, A.J.; Kempton, J.W.; Wilde, S.B. The association of algicidal bacteria and raphidophyte blooms in South Carolina brackish detention ponds. *Harmful Algae* **2008**, *7*, 184–193. [CrossRef]
18. Zhang, F.; Ye, Q.; Chen, Q.; Yang, K.; Zhang, D.; Chen, Z.; Lu, S.; Shao, X.; Fan, Y.; Yao, L.; et al. Algicidal activity of novel marine bacterium *Paracoccus* sp. strain Y42 against a harmful algal-bloom-causing dinoflagellate, *Prorocentrum donghaiense*. *Appl. Environ. Microbiol.* **2018**, *84*, e01015-18. [CrossRef]
19. Matcher, G.; Lemley, D.A.; Adams, J.B. Bacterial community dynamics during a harmful algal bloom of *Heterosigma akashiwo*. *Aquat. Microb. Ecol.* **2021**, *86*, 153167. [CrossRef]
20. Zhou, J.; Richlen, M.L.; Sehein, T.R.; Kulis, D.M.; Anderson, D.M.; Cai, Z. Microbial community structure and associations during a marine dinoflagellate bloom. *Front. Microbiol.* **2018**, *9*, 1201. [CrossRef]
21. Buchan, A.; LeCleir, G.R.; Gulvik, C.A.; Gonzalez, J.M. Master recyclers: Features and functions of bacteria associated with phytoplankton blooms. *Nat. Rev. Microbiol.* **2014**, *12*, 686–698. [CrossRef]
22. Abdennadher, M.; Hamza, A.; Fekih, W.; Hannachi, I.; Bellaaj, A.Z.; Bradai, M.N.; Aleya, L. Factors determining the dynamics of toxic blooms of *Alexandrium minutum* during a 10-year study along the shallow southwestern Mediterranean coasts. *Estuar. Coast. Shelf Sci.* **2012**, *106*, 102–111. [CrossRef]
23. Feki, W.; Hamza, A.; Frossard, V.; Abdennadher, M.; Hannachi, I.; Jacquot, M.; Bel Hassen, M.; Aleya, L. What are the potential drivers of blooms of the toxic dinoflagellate *Karenia selliformis*? A 10-year study in the Gulf of Gabes, Tunisia, southwestern Mediterranean Sea. *Harmful Algae.* **2013**, *23*, 8–18. [CrossRef]
24. Daly Yahia-Kefi, O.; Daly Yahia, M.N. Le phytoplancton toxique dans trois milieux lagunaires tunisiens (Ghar El Melh, Lac Sud de Tunis et Bou Ghrara). In *Actes Séminaire National sur la Gestion et la Conservation des Zones Humides Tunisiennes*; The Minister of Agriculture: Tunis, Tunisia, 1997; pp. 27–29.
25. Romdhane, M.S.; Eilertsen, H.C.; Daly Yahia-Kéfi, O.; Daly Yahia, M.N. Toxic dinoflagellate blooms in Tunisian lagoons: Causes and consequences for aquaculture. In *Harmful Algae*; Reguera, B., Blanco, J., Fernandez, M.L., Wyatt, T., Eds.; Intergovernmental Oceanographic Commission of UNESCO: Paris, France, 1998; pp. 80–83.
26. Daly Yahia-Kéfi, O.; Souissi, S.; Gómez, F.; Daly Yahia, M.N. Spatio-temporal distribution of the dominant diatom and dinoflagellate species in the Bay of Tunis (SW Mediterranean Sea). *Mediterr. Mar. Sci.* **2005**, *6*, 17–34. [CrossRef]
27. Armi, Z.; Milandri, M.; Turki, S.; Hajjem, B. *Alexandrium catenella* and *Alexandrium tamarense* in the North Lake of Tunis: Bloom characteristics and occurrence of paralytic shellfish toxin. *Afr. J. Aquat. Sci.* **2011**, *36*, 36–41. [CrossRef]
28. Turki, S.; Dhib, A.; Fertouna-Bellakhal, M.; Frossard, V.; Balti, N.; Kharrat, R.; Aleya, L. Harmful algal blooms (HABs) associated with phycotoxins in shellfish: What can be learned from five years of monitoring in Bizerte Lagoon (Southern Mediterranean Sea)? *Ecol. Eng.* **2014**, *67*, 39–347. [CrossRef]
29. Sammari, C.; Koutitonsky, V.G.; Moussa, M. Sea level variability and tidal resonance in the Gulf of Gabes, Tunisia. *Cont. Shelf Res.* **2006**, *26*, 338–350. [CrossRef]
30. Chifflet, S.; Tedetti, M.; Zouch, H.; Fourati, R.; Zaghden, H.; Elleuch, B.; Quéméneur, M.; Karray, F.; Sayadi, S. Dynamics of trace metals in a shallow coastal ecosystem: Insights from the Gulf of Gabès (southern Mediterranean Sea). *AIMS Environ. Sci.* **2019**, *6*, 277–297. [CrossRef]
31. Zaghden, H.; Tedetti, M.; Sayadi, S.; Serbaji, M.M.; Elleuch, B.; Saliot, A. Origin and distribution of hydrocarbons and organic matter in the surficial sediments of the Sfax-Kerkennah channel (Tunisia, Southern Mediterranean Sea). *Mar. Pollut. Bull.* **2017**, *117*, 414–428. [CrossRef] [PubMed]
32. Utermöhl, H. Zur Vervolkommung der quantitativen Phytoplankton-methodik. *Comm. Assoc. Int. Limnol. Theor. Appl.* **1958**, *9*, 1–38. [CrossRef]
33. Throndsen, J. Estimating cell numbers. In *Manual on Harmful Marine Microalgae*; Hallegraeff, G.M., Anderson, D.M., Cembella, A.D., Enevoldsen, H.O., Eds.; IOCManual and Guides 33; UNESCO: Paris, France, 1995; pp. 63–80.
34. Anderson, D.M.; Kulis, D.M.; Keafer, B.A.; Gribble, K.E.; Marin, R.; Scholin, C.A. Identification and enumeration of *Alexandrium* spp. from the Gulf of Maine using molecular probes. *Deep Sea Res. Part II* **2005**, *52*, 19–21. [CrossRef]
35. Guillard, R.R.L.; Hargraves, P.E. *Stichochrysis immobilis* is a diatom, not a chrysophyte. *Phycologia* **1993**, *32*, 234–236. [CrossRef]

36. Balech, E. *The Genus Alexandrium Halim (Dinoflagellata)*; Sherkin Island Marine Station, Sherkin Island, Co.: Cork, Ireland, 1995; p. 151.
37. Fritz, L.; Triemer, R.E. A rapid simple technique utilizing calcofluor white M2R for the visualization of dinoflagellates thecal plates. *J. Phycol.* **1985**, *21*, 662–664. [CrossRef]
38. Tréguer, P.; Le Corre, P. *Manuel d'analyse des sels nutritifs dans l'eau de mer*; Université de Bretagne Occidentale: Brest, France, 1975; 110p.
39. Takahashi, S.; Tomita, J.; Nishioka, K.; Hisada, T.; Nishijima, M. Development of a prokaryotic universal primer for simultaneous analysis of *Bacteria* and *Archaea* using next-generation sequencing. *PLoS ONE* **2014**, *9*, e105592. [CrossRef] [PubMed]
40. Dowd, S.E.; Callaway, T.R.; Wolcott, R.D.; Sun, Y.; McKeehan, T.; Hagevoort, R.G.; Edrington, T.S. Evaluation of the bacterial diversity in the feces of cattle using 16S rDNA bacterial tag-encoded FLX amplicon pyrosequencing (bTEFAP). *BMC Microbiol.* **2008**, *8*, 125. [CrossRef] [PubMed]
41. Adachi, M.; Sako, Y.; Ishida, Y. Restriction fragment length polymorphism of ribosomal DNA internal transcribed spacer and 5.8S regions in Japanese *Alexandrium* species (*Dinophyceae*). *J. Phycol.* **1994**, *30*, 857–863. [CrossRef]
42. Leaw, C.P.; Lim, P.T.; Ahmad, A.; Usup, G. Genetic diversity of *Ostreopsis ovata* (Dinophyceae) from Malaysia. *Mar. Biotechnol.* **2001**, *3*, 246–255.
43. Scholin, C.A.; Herzog, M.; Sogin, M.; Anderson, D.M. Identification of group- and strain-specific genetic markers for globally distributed *Alexandrium* (Dinophyceae). II. Sequence analysis of a fragment of the LSU rRNA gene. *J. Phycol.* **1994**, *30*, 999–1011. [CrossRef]
44. Abdennadher, M.; Bellaaj Zouari, A.; Medhioub, W.; Penna, A.; Hamza, A. Characterization of *Coolia* spp. (Gonyaucales, Dinophyceae) from Southern Tunisia: First record of *Coolia malayensis* in the Mediterranean Sea. *Algae* **2021**, *6*, 175–193. [CrossRef]
45. Halim, Y. *Alexandrium minutum* nov. g. nov. sp. Dinoflagellate provocant des "eaux rouges". *Vie et Milieu.* **1960**, *11*, 102–105.
46. Smythe-Wright, D.; Daniel, A.; Boswell, S.; Purcell, D.; Hartman, M.; Hartman, S. Phytoplankton and pigment studies in the Bay of Biscay and English Channel. *Deep Sea Res. Part II* **2014**, *106*, 76–86. [CrossRef]
47. Tas, S.; Yilmaz, I.N. Potentially harmful microalgae and algal blooms in a eutrophic estuary in Turkey. *Mediterr. Mar. Sci.* **2015**, *16*, 432–443. [CrossRef]
48. Daly Yahia-Kefi, O.; Nézan, E.; Daly Yahia, M.N. Sur la présence du genre *Alexandrium halim* (Dinoflagellés) dans la baie de Tunis (Tunisie). *Oceanol. Acta.* **2001**, *24*, 17–25. [CrossRef]
49. Fraga, S.; Bravo, I.; Delgado, M.; Franco, J.M.; Zapata, M. *Gyrodinium impudicum* sp. nov. (Dinophyceae), a non-toxic, chain forming, red tide dinoflagellate. *Phycologia* **1995**, *34*, 514–521. [CrossRef]
50. Luo, Z.; Hu, Z.; Tang, Y.; Mertens, K.N.; Leaw, C.P.; Lim, P.T.; Teng, S.T.; Wang, L.; Gu, H. Morphology, ultrastructure, and molecular phylogeny of *Wangodinium sinense* gen. et sp. nov. (Gymnodiniales, Dinophyceae) and revisiting of Gymnodinium dorsalisulcum and Gymnodinium impudicum. *J. Phycol.* **2018**, *54*, 744. [CrossRef]
51. Ranston, E.R.; Webber, D.F.; Larsen, J. The first description of the potentially toxic dinoflagellate, *Alexandrium minutum* in Hunts Bay, Kingston Harbour, Jamaica. *Harmful Algae* **2007**, *6*, 29–47. [CrossRef]
52. Touzet, N.; Farrell, H.; Rathaille, A.N.; Rodriguez, P.; Alfonso, A.; Botana, L.M.; Raine, R. Dynamics of co-occurring *Alexandrium minutum* (Global Clade) and *A. tamarense* (West European) (Dinophyceae) during a summer bloom in Cork Harbour, Ireland (2006). *Deep Sea Res. Part II* **2010**, *57*, 268–278. [CrossRef]
53. Labib, G.; Halim, Y. Diel vertical migration toxicity of *Alexandrium minutum* Halim red tide, in Alexandria. *Egypt. Mar. Life* **1995**, *5*, 11–17.
54. Delgado, M.; Estrada, M.; Camp, J.; Fernandez, J.V.; Santmarti, M.; Lleti, C. Development of a toxic *Alexandrium minutum* Halim (Dinophyceae) bloom in the harbour of Sant Carles de la Ràpita (Ebro delta, northwestern Mediterranean). *Scient. Mar.* **1990**, *54*, 1–7.
55. Garcés, E.; Bravo, I.; Vila, M.; Figueroa, R.I.; Maso, M.; Sampedro, N. Relationship between vegetative cells and cyst production during *Alexandrium minutum* bloom in Arenys de Mar harbor (NW Mediterranean). *J. Plankton Res.* **2004**, *26*, 637–645. [CrossRef]
56. Chapelle, A.; Le Gac, M.; Labry, C.; Siano, R.; Quere, J.; Caradec, F.; Le Bec, C.; Nezan, E.; Doner, A.; Gouriou, J. The Bay of Brest (France), a new risky site for toxic *Alexandrium minutum* blooms and PSP shellfish contamination. *Harmful Algae News* **2015**, *51*, 4–5.
57. Cosgrove, S.; Rathaille, A.N.; Raine, R. The influence of bloom intensity on the encystment rate and persistence of *Alexandrium minutum* in Cork harbor, Ireland. *Harmful Algae* **2014**, *31*, 114–124. [CrossRef]
58. Guallar, C.; Bacher, C.; Chapelle, A. Global and local factors driving the phenology of *Alexandrium minutum* (Halim) blooms and its toxicity. *Harmful Algae* **2017**, *67*, 44–60. [CrossRef] [PubMed]
59. Maguer, J.F.; Wafar, M.; Madec, C.; Morin, P.; Erard-Le Denn, E. Nitrogen and phosphorus requirements of an *Alexandrium minutum* bloom in the Penze estuary, France. *Limnol. Oceanogr.* **2004**, *49*, 1108–1114. [CrossRef]
60. Pitcher, G.C.; Cembella, A.D.; Joyce, L.B.; Larsen, J.; Probyn, T.A.; Ruiz Sebastian, C. The dinoflagellate *Alexandrium minutum* in Cape Town harbor (South Africa): Bloom characteristics, phylogenetic analysis and toxin composition. *Harmful Algae* **2007**, *6*, 823–836. [CrossRef]
61. Santos, M.; Costa, P.R.; Porteiro, F.M.; Moita, M.T. First report of a massive bloom of *Alexandrium minutum* (Dinophyceae) in middle North Atlantic: A coastal lagoon in S. Jorge Island, Azores. *Toxicon* **2014**, *90*, 265–268. [CrossRef]

62. Mikhail, S.; Khalil, N.; El-Hadary, M. A new recorded of red tide forming species; *Heterocapsa triquetra*, *Gymnodinium impudicum*, *Heterosigma akashiwo* and *Thalassiosira rotula* in Alexandria waters, Egypt. *Egypt. J. Aquat. Biol. Fish.* **2020**, *24*, 207–223. [CrossRef]
63. Bravo, I.; Vila, M.; Maso, M.; Figueroa, R.I.; Ramilo, I. *Alexandrium catenella* and *Alexandrium minutum* blooms in the Mediterranean Sea: Toward the identification of ecological niches. *Harmful Algae* **2008**, *7*, 515–522. [CrossRef]
64. Grzebyk, D.; Bechemin, C.; Ward, C.J.; Verite, C.; Codd, G.A.; Maestrini, S.Y. Effects of salinity and two coastal waters on the growth and toxin content of the dinoflagellate *Alexandrium minutum*. *J. Plankton Res.* **2003**, *25*, 1185–1199. [CrossRef]
65. Lim, P.T.; Ogata, T. Salinity effect on growth and toxin production of four tropical *Alexandrium* species (Dinophyceae). *Toxicon* **2005**, *45*, 699–710. [CrossRef]
66. Hwang, D.F.; Lu, Y.H. Influence of environmental and nutritional factors on growth, toxicity, and toxin profile of dinoflagellate *Alexandrium minutum*. *Toxicon* **2000**, *38*, 1491–1503. [CrossRef] [PubMed]
67. Flores-Moya, A.; Rouco, M.; García-Sánchez, M.J.; García-Balboa, C.; González, R.; Costas, E.; López Rodas, V. Effects of adaptation, chance, and history on the evolution of the toxic dinoflagellate *Alexandrium minutum* under selection of increased temperature and acidification. *Ecol. Evol.* **2012**, *2*, 1251–1259. [CrossRef] [PubMed]
68. Maguer, J.F.; L'Helguen, S.; Madec, C.; Labry, C.; Le Corre, P. Nitrogen uptake and assimilation kinetics in *Alexandrium minutum* (Dynophyceae): Effect of N-limited growth rate on nitrate and ammonium interactions. *J. Phycol.* **2007**, *43*, 295303. [CrossRef]
69. Giacobbe, M.G.; Oliva, F.D.; Maimone, G. Environmental factors and seasonal occurrence of the dinoflagellate *Alexandrium minutum*, a PSP potential producer, in a Mediterranean Lagoon. *Estuar. Coast. Shelf Sci.* **1996**, *42*, 539–549. [CrossRef]
70. Le Bec, C.; Legendre, A.; Messiaen, G. Changes in the annual harmful algal blooms of *Alexandrium minutum*: Effects of environmental conditions and drainage basin inputs in the Rance estuary (Brittany, France). *Aquat. Living Resour.* **2016**, *29*, 104. [CrossRef]
71. Carrada, G.C.; Casotti, R.; Modigh, M.; Saggiomo, V. Presence of *Gymnodinium catenatum* (Dinophyceae) in a coastal Mediterranean lagoon. *J. Plankton Res.* **1991**, *13*, 229–238. [CrossRef]
72. Friligos, N.; Gotsis-Skretas, O. Eutrophisation and red tide in Aegean coastal waters. *Toxicol. Environ. Chem.* **1989**, *20*, 171–180. [CrossRef]
73. Oh, S.J.; Hyeon, K.K.; Hyeon, N.; Han-Soe, Y. Dissolved organic phosphorus utilization and alkaline phosphatase activity of the dinoflagellate *Gymnodinium impudicum* isolated from the South Sea of Korea. *Ocean Sci. J.* **2010**, *45*, 171–178. [CrossRef]
74. Vautard, R.; Cattiaux, J.; You, P.; Thépaut, J.-N.; Ciais, P. Northern Hemisphere atmospheric stilling partly attributed to an increase in surface roughness. *Nat. Geosci.* **2010**, *3*, 756. [CrossRef]
75. Deng, J.M.; Zhang, Y.L.; Qin, B.Q.; Shi, K. Long-term changes in surface solar radiation and their effects on air temperature in the Shanghai region. *Int. J. Climatol.* **2015**, *35*, 3385–3396. [CrossRef]
76. Deng, J.; Paerl, H.W.; Qin, B.; Zhang, Y.; Zhu, G.; Jeppesen, E.; Cai, Y.; Xu, H. Climatically modulated decline in wind speed may strongly affect eutrophication in shallow lakes. *Sci. Total. Environ.* **2018**, *645*, 1361–1370. [CrossRef] [PubMed]
77. Brody, S.R.; Lozier, M. Changes in dominant mixing length scales as a driver of subpolar phytoplankton bloom initiation in the North Atlantic. *Geophys. Res. Lett.* **2014**, *41*, 3197–3203. [CrossRef]
78. Brody, S.R.; Lozier, M.S. Characterizing upper-ocean mixing and its effect 603 on the spring phytoplankton bloom with in situ data. ICES. *J. Mar. Sci.* **2015**, *72*, 1961–1970. [CrossRef]
79. Pellichero, V.; Boutin, J.; Claustre, H.; Merlivat, L.; Sallée, J.B.; Blain, S. Relaxation of wind stress drives the abrupt onsetof biological carbon uptake in the Kerguelen bloom: A multisensor approach. *Geophys. Res. Lett.* **2020**, *47*, e2019GL085992. [CrossRef]
80. Merlivat, L.; Hemming, M.; Boutin, J.; Antoine, D.; Vincenzo Vellucci, V.; Golbol, M.; Lee, G.A.; Beaumon, L. Physical mechanisms for biological carbon uptake during the onset of the spring phytoplankton bloom in the northwestern Mediterranean Sea (BOUSSOLE site). *Biogeosciences* **2022**, *19*, 3911–3920. [CrossRef]
81. Matteson, A.R.; Loar, S.N.; Pickmere, S.; DeBruyn, J.M.; Ellwood, M.J.; Boyd, P.W.; Hutchins, D.A.; Wilhelm, S.W. Production of viruses during a spring phytoplankton bloom in the South Pacific Ocean near of New Zealand. *FEMS Microbiol. Ecol.* **2012**, *79*, 709–719. [CrossRef]
82. Kim, Y.S.; Son, H.J.; Jeong, S.Y. Isolation of an algicide from a marine bacterium and its effects against the toxic dinoflagellate *Alexandrium catenella* and other harmful algal bloom species. *J. Microbiol.* **2015**, *53*, 511–517. [CrossRef] [PubMed]
83. Needham, D.M.; Fuhrman, J.A. Pronounced daily succession of phytoplankton, archaea and bacteria following a spring bloom. *Nat. Microbiol.* **2016**, *1*, 16005. [CrossRef]
84. Rink, B.; Seeberger, S.; Martens, T.; Duerselen, C.D.; Simon, M.; Brinkhoff, T. Effects of phytoplankton bloom in a coastal ecosystem on the composition of bacterial communities. *Aquat. Microb. Ecol.* **2007**, *48*, 47–60. [CrossRef]
85. Li, Z.; Li, L.; Song, K.; Cassar, N. Estimation of phytoplankton size fractions based on spectral features of remote sensing ocean color data. *J. Geophys. Res. Ocean.* **2013**, *118*, 1445–1458. [CrossRef]
86. Fandino, L.B.; Riemann, L.; Steward, G.F.; Long, R.A.; Azam, F. Variations in bacterial community structure during dinoflagellate bloom analyzed by DGGE and 16S rDNA sequencing. *Aquat. Microb. Ecol.* **2001**, *23*, 119–130. [CrossRef]
87. Quéméneur, M.; Bel Hassen, M.; Armougom, F.; Khammeri, Y.; Lajnef, R.; Bellaaj-Zouari, A. Prokaryotic diversity and distribution along physical and nutrient gradients in the Tunisian coastal waters (South Mediterranean Sea). *Front. Microbiol.* **2020**, *11*, 593540. [CrossRef] [PubMed]

88. Pernthaler, A.; Pernthaler, J.; Amann, R. Fluorescence in situ hybridization and catalyzed reporter deposition for the identification of marine bacteria. *Appl. Environ. Microbiol.* **2002**, *68*, 661–667. [CrossRef] [PubMed]
89. Lima-Mendez, G.; Faust, K.; Henry, N.; Decelle, J.; Colin, S.; Carcillo, F. Determinants of community structure in the global planktoninteractome. *Science* **2015**, *348*, 1262073. [CrossRef]
90. Martin-Cuadrado, A.B.; Garcia-Heredia, I.; Moltó, A.G.; López-Úbeda, R.; Kimes, N.; López-García, P.; Moreira, D.; Rodriguez-Valera, F. A new class of marine Euryarchaeota group II from the mediterranean deep chlorophyll maximum. *ISME J.* **2015**, *9*, 1619–1634. [CrossRef] [PubMed]
91. Hugoni, M.; Taib, N.; Debroas, D. Structure of the rare archaeal biosphere and seasonal dynamics of active ecotypes in surface coastal waters. *Proc. Natl. Acad. Sci. USA* **2013**, *110*, 6004–6009. [CrossRef] [PubMed]
92. Garcés, E.; Vila, M.; Reñé, A.; Alonso-Sáez, L.; Anglès, S.; Lugliè, A.; Masó, M.; Gasol, J.M. Natural bacterioplankton assemblage composition during blooms of *Alexandrium* spp. (*Dinophyceae*) in NW Mediterranean coastal waters. *Aquat. Microb. Ecol.* **2007**, *46*, 55–70. [CrossRef]
93. Jasti, S.; Sieracki, M.E.; Poulton, N.J.; Giewat, M.W.; Rooney-Varga, J.N. Phylogenetic diversity and specificity of bacteria closely associated with *Alexandrium spp*. and other phytoplankton. *Appl. Environ. Microbiol.* **2005**, *71*, 3483–3494. [CrossRef]
94. Zouch, H.; Karray, F.; Armougom, F.; Chifflet, S.; Hirschler-Réa, A.; Kharrat, H.; Kamoun, L.; Ben Hania, W.; Ollivier, B.; Sayadi, S.; et al. Microbial diversity in sulfate-reducing marine sediment enrichment cultures associated with anaerobic biotransformation of coastal stockpiled phosphogypsum (Sfax, Tunisia). *Front. Microbiol.* **2017**, *8*, 1583. [CrossRef] [PubMed]
95. Zouch, H.; Cabrol, L.; Chifflet, S.; Tedetti, M.; Karray, F.; Zaghden, H.; Sayadi, S.; Quéméneur, M. Effect of acidic industrial effluent release on microbial diversity and trace metal dynamics during resuspension of coastal sediment. *Front. Microbiol.* **2018**, *9*, 3103. [CrossRef] [PubMed]
96. Hiraishi, A.; Nagao, N.; Yonekawa, C.; Umekage, S.; Kikuchi, Y.; Eki, T.; Hirose, Y. Distribution of phototrophic purple nonsulfur bacteria in massive blooms in coastal and wastewater ditch environments. *Microorganisms* **2020**, *8*, 150. [CrossRef] [PubMed]
97. Caumette, P.; Baleux, B. Etude des eaux rouges dues à la prolifération des bactéries photosynthétiques sulfo-oxydantes dans l'étang du Prévost, lagune saumâtre méditerranéenne. *Mar. Biol.* **1980**, *56*, 183–194. [CrossRef]
98. Caumette, P. Phototrophic sulfur bacteria and sulfate-reducing bacteria causing red waters in a shallow brackish coastal lagoon (Prévost Lagoon, France). *FEMS. Microbiol. Lett.* **1986**, *38*, 113–124. [CrossRef]
99. Belila, A.; Abbas, B.; Fazaa, I.; Saidi, N.; Snoussi, M.; Hassen, A.; Muyzer, G. Sulfur bacteria in wastewater stabilization ponds periodically affected by the red-water phenomenon. *Appl. Microbiol. Biotechnol.* **2013**, *97*, 379–394. [CrossRef] [PubMed]
100. Hampton, S.E.; Gray, D.K.; Izmest'eva, L.R.; Moore, M.V.; Ozersky, T. The rise and fall of plankton: Long-term changes in the vertical distribution of algae and grazers in Lake Baikal, Siberia. *PLoS ONE* **2014**, *9*, e88920. [CrossRef] [PubMed]
101. Frenken, T.; Velthuis, M.; de Senerpont Domis, L.N.; Stephan, S.; Aben, R.; Kosten, S.; van Donk, E.; Van de Waal, D.B. Warming accelerates termination of a phytoplankton spring bloom by fungal parasites. *Glob Chang. Biol.* **2016**, *22*, 299–309. [CrossRef] [PubMed]